

PREPARED FOR SUBMISSION TO JCAP

No WIMP Mini-Spikes in Dwarf Spheroidal Galaxies

Mark Wanders,^a Gianfranco Bertone,^a Marta Volonteri,^b and Christoph Weniger^a

^aGRAPPA, University of Amsterdam,
Science Park 904, Amsterdam, the Netherlands

^bInstitut d'Astrophysique de Paris,
98bis Boulevard Arago, Paris, France

Abstract. The formation of black holes inevitably affects the distribution of dark and baryonic matter in their vicinity, leading to an enhancement of the dark matter density, called *spike*, and if dark matter is made of WIMPs, to a strong enhancement of the dark matter annihilation rate. Spikes at the center of galaxies like the Milky Way are efficiently disrupted by baryonic processes, but *mini-spikes* can form and survive undisturbed at the center of dwarf spheroidal galaxies. We show that *Fermi* LAT satellite data allow to set very stringent limits on the existence of mini-spikes in dwarf galaxies: for thermal WIMPs with mass between 100 GeV and 1 TeV, we obtain a maximum black hole mass between 100 and 1000 M_{\odot} , ruling out black holes masses extrapolated from the M - σ relationship in a large region of the parameter space. We also performed Monte Carlo simulations of merger histories of black holes in dwarf spheroidals in a scenario where black holes form from the direct collapse of primordial gas in early halos, and found that this specific formation scenario is incompatible at the 84% CL with dark matter being in the form of thermal WIMPs.

Contents

1	Introduction	1
2	Mini-spikes	2
2.1	Dwarf spheroidals	2
2.2	Gamma-rays from DM annihilation	3
2.3	Intermediate mass black holes	4
2.4	DM spiked density profile and annihilation rate	5
2.5	Persistence of the mini-spike	7
3	Intermediate mass black holes in dwarf spheroidals	8
3.1	Monte Carlo simulation of merger histories	8
3.1.1	IMBHs in dwarf spheroidals of the Milky Way and M31	9
3.2	Other limits on the black hole mass	11
3.2.1	SMBH-host galaxy relations and substructure considerations	11
3.2.2	Kinematic measurements	11
4	<i>Fermi</i> LAT analysis	12
4.1	Data reduction and statistical method	12
4.2	Results for Draco	14
4.2.1	Flux and cross section upper limits	14
4.2.2	Black hole mass upper limit	14
4.3	Other dwarf spheroidal galaxies	16
5	Conclusions	17

1 Introduction

In most scenarios that lead to the formation of supermassive black holes (SMBHs, $M_{\bullet} \sim 10^6\text{--}10^8 M_{\odot}$), the growth of these objects from a small seed inevitably affects the distribution of baryonic matter around them (e.g. refs. [1, 2]) and can lead to large overdensities in the dark matter (DM) [3] distribution called *spikes* [4]. If DM is made of Weakly Interacting Massive Particles (WIMPs) [5–7], these overdensities imply a strong enhancement of the DM annihilation rate at the Galactic center [4, 8–10] and more in general around any SMBH, boosting the predicted extragalactic gamma-ray background [11, 12]. However, mergers, off-center formation of the seed black holes (BHs) and gravitational scattering off of stars are likely to disrupt spikes at the center of galaxies like the Milky Way (MW) [13–15].

These overdensities would instead persist around intermediate mass black holes (IMBHs), objects whose size falls between that of stellar and SMBHs, in the range $10^2\text{--}10^6 M_{\odot}$. IMBHs are a generic prediction of SMBHs scenarios, and for which compelling

evidence has been recently obtained [16]. Mini-spikes around IMBHs are interesting targets for indirect DM searches, based on the search for secondary particles, like gamma-rays, neutrinos and anti-matter, produced by the annihilation of WIMPs [7, 17–23]. IMBHs may be in particular hosted at the center of dwarf spheroidal galaxies in the MW halo. Dynamical constraints on their mass are rather loose, due to the paucity of stars in these systems, but tentative estimates can be obtained by extrapolating astrophysical relationships between the mass of SMBHs and the properties of the host halos (e.g. ref. [24]).

We study here the enhancement of the DM annihilation rate produced by the formation of BHs at the center of dwarf spheroidal galaxies under the assumption that the DM is made of WIMPs. We show that the lack of excess photons from dwarf spheroidal galaxies in *Fermi* LAT satellite data allow to set very stringent limits on mini-spikes in these astrophysical structures, and estimate the maximum mass of black holes producing them as a function of WIMP mass (for another recent analysis that instead concentrates on constraining WIMP DM models see ref. [68]).

We also perform Monte Carlo simulations of merger histories of black holes in dwarf spheroidals in a scenario where black holes form the direct collapse of primordial gas in early halos, and show that this specific formation scenario is incompatible at the 84% CL with dark matter being in the form of thermal WIMPs.

The article is organized as follows: in section 2 we discuss the DM enhancement produced by the formation of a black hole at the center of dwarf galaxies; in section 3 we discuss our simulations of IMBHs in dwarf galaxies and existing limits; in section 4 we present the *Fermi* data we used, our analysis technique and its results and we present our conclusions in section 5.

2 Mini-spikes

2.1 Dwarf spheroidals

Dwarf spheroidal galaxies (dSphs) are low luminosity ($L = 10^3 - 10^8 L_\odot$ compared to $L \sim 2 \times 10^{10} L_\odot$ for a normal galaxy) objects orbiting the MW with masses within their half-light radius on the order of $10^5 - 10^7 M_\odot$ [25]. They are the largest galactic substructures predicted in the cold DM model and ideal laboratories for DM indirect detection, for various reasons. They are largely DM dominated systems, as shown by their high mass-to-light ratios ($M/L \sim 100 - 1000 M_\odot/L_\odot$ [26]). This allows the use of stars as trace-particles of the DM gravitational potential and thus constraints on the DM distribution can be derived from stellar kinematics. Moreover, dSphs contain no detected neutral or ionized gas and show little to no star formation activity [27–29], which would simplify the interpretation of the detection of a gamma-ray excess in the direction of a dSph.

We choose as an illustrative example the Draco dSph, as it has the highest expected J -factor of all the Local Group’s dSph satellites (see also table 1). Additionally, its relatively high galactic latitude ($b = 57.9^\circ$) makes contamination by other gamma-ray sources in the galactic disk unlikely. Deep photometric studies of Draco indicate it is

unaffected by Galactic tides [30], which supports our assumption (see next subsection) of a simple power-law density profile as well as disfavors the possible disruption of a mini-spike by Galactic tidal forces or merger events.

Name	D (kpc)	r_s (kpc)	ρ_s ($10^8 M_\odot/\text{kpc}^3$)	$J_{\text{NFW}} \left(10^{19} \frac{\text{GeV}^2}{\text{cm}^5}\right)$
Bootes I	62 ± 3	0.27	2.04	$0.16^{+0.35}_{-0.13}$
Coma Berenices	44 ± 4	0.16	2.57	$0.16^{+0.22}_{-0.08}$
Draco	76 ± 5	2.09	0.26	$1.20^{+0.31}_{-0.25}$
Fornax	138 ± 8	0.58	0.66	$0.06^{+0.03}_{-0.03}$
Sculptor	79 ± 4	0.95	0.37	$0.24^{+0.06}_{-0.06}$
Sextans	86 ± 4	0.37	0.85	$0.06^{+0.03}_{-0.02}$
Ursa Major II	30 ± 5	0.65	0.98	$0.58^{+0.91}_{-0.35}$
Ursa Minor	66 ± 3	0.17	3.47	$0.64^{+0.25}_{-0.18}$

Table 1: Properties of dSphs in the Milky Way halo with the highest expected J-factors, from ref. [26]. Here, D is the distance, r_s and ρ_s are respectively the scale radius and density and J_{NFW} is the J -factor for a solid angle of 2.4×10^{-4} sr and an NFW profile.

2.2 Gamma-rays from DM annihilation

The density profile of is often approximated with a so-called Navarro, Frenk and White (NFW) profile [31]:

$$\rho(r) = \frac{r_s^3 \rho_s}{r(r + r_s)^2}, \quad (2.1)$$

where r_s and ρ_s are the scale radius and scale density, respectively, and for Draco we take the values $r_s = 2.09 \text{ kpc}$ and $\rho_s = 10^{7.41} M_\odot/\text{kpc}^3 \cong 0.976 \text{ GeV}/\text{cm}^3$ [26]. We will discuss below how our results depend on this specific assumption. For a self-annihilating DM particle and fixed gamma-ray energy spectrum, the gamma-ray flux from annihilation scales with ρ^2 , specifically $\Phi \propto \frac{\langle \sigma v \rangle}{m_\chi^2} J$, where m_χ is the mass of the WIMP, $\langle \sigma v \rangle$ is its cross section (assumed to be velocity independent) and the J -factor is defined as the integral of the DM density ρ_{DM} squared over the line of sight l ,

$$J = \int_{l.o.s.} \rho_{DM}^2 dl. \quad (2.2)$$

In this case, however, we are interested in the averaged flux over a region $\Delta\Omega$ and thus the gamma-ray flux is given by

$$\frac{d\Phi}{dE}(\Delta\Omega) = \frac{1}{2} \frac{dN_\gamma}{dE} \frac{\langle \sigma v \rangle}{m_\chi^2} \frac{\bar{J}(\Delta\Omega)}{4\pi}, \quad (2.3)$$

where $\bar{J}(\Delta\Omega)$ is the average J-factor for a region of $\Delta\Omega$, and dN_γ/dE is the photon energy spectrum.

2.3 Intermediate mass black holes

So far, the most convincing observational evidence for the existence of IMBHs is in the form of the so called ultra-luminous X-ray sources (ULXs). These are extragalactic, non-nuclear sources of X-ray radiation with isotropic luminosities in the 0.3–10 keV band of $L_X > 10^{39} \text{ erg s}^{-1}$, exceeding those of stellar mass black holes accreting at the Eddington rate (e.g. [32]). Recently, the existence of a $400 M_\odot$ IMBH powering the X-ray source M82 X-1 has been reported in ref. [16]. Several theoretical motivations for the existence of IMBHs have also been raised. Strong empirical correlations between the mass of SMBHs and the properties of their host galaxies suggest an inherent connection between the growth of the SMBH and the formation and evolution of galaxies. Extending these relations down to low-mass galaxies predicts the presence of IMBHs in their centers [24]. Additionally, they have been proposed as the initial seeds of SMBHs (see e.g. [33]).

We now briefly review two proposed formation scenarios for IMBHs discussed in ref. [34]. In the first, scenario popIII, black holes form after the collapse of population III stars. The second scenario pGas features black holes originating from massive objects formed directly during the collapse of primordial gas in early-forming halos.

Scenario popIII

The evolution and eventual fate of massive stars with zero metallicity differs significantly from those of their metal-enriched equivalents [35]. Pop I main sequence stars with masses over $100 M_\odot$ are vibrationally unstable to radial pulsations, leading to substantial mass loss, an effect which is substantially suppressed in low metallicity massive stars. This, combined with the fact that, at zero metallicity, mass loss through stellar winds is also negligible, means that massive Pop III stars could reach the end of their life with a mass close to their initial mass.

However, whereas zero metallicity stars with masses in the range $M_\bullet \sim 60\text{--}140 M_\odot$ and $M_\bullet \geq 260 M_\odot$ collapse directly into black holes, those with masses between $140 \leq M/M_\odot \leq 260$ will explode in a pair-instability supernova, leaving behind no remnant [36].

Scenario pGas

As the first halos virialize and collapse, gas cools and collapses as well, forming pressure-supported disks at the center of those halos massive enough to contain sufficient amounts of molecular hydrogen. If molecular hydrogen cooling is efficient and no major mergers occur over a dynamical time, a protogalactic disk can form. Gravitational instabilities in the disk produce an effective viscosity that transfer angular momentum outwards and mass inwards. By the time this process is halted by the heating of the disk by supernovae of Pop III stars, a baryonic mass on the order of $\sim 10^5 M_\odot$ has been transferred to the center of the disk [37]. Such an object may be temporarily pressure supported, but will inevitably collapse into a black hole [36, 38].

In both scenarios, the initial black hole forms and grows on timescales long enough to ensure adiabaticity [34]. This causes the surrounding DM halo to contract, resulting in a mini-spike in the density profile. However, the mini-spike is unlikely to survive in the case of off-center (relative to the DM halo) IMBH formation (i.e. scenario popIII), as we discuss in section 2.5. Thus, we are mostly interested in scenario pGas.

2.4 DM spiked density profile and annihilation rate

We will first consider the radius of the gravitational influence of the black hole r_h , which is the radius at which the enclosed mass equals twice the black hole mass [34]:

$$M(< r_h) \equiv \int_0^{r_h} \rho_{DM}(r) 4\pi r^2 dr = 2M_\bullet, \quad (2.4)$$

where ρ_{DM} is the density of DM. For an arbitrary power law $\rho(r) = \rho_s (r/r_s)^{-\gamma}$, from eq. (2.4) it follows that

$$r_h = r_s \left(\frac{3-\gamma}{2\pi} \frac{M_\bullet}{\rho_s r_s^3} \right)^{1/(3-\gamma)}. \quad (2.5)$$

For Draco, we can consider both the enclosed mass from the DM in the NFW profile as well as the enclosed stellar mass, and so eq. (2.4) becomes

$$M(< r_h) \equiv \int_0^{r_h} [\rho_*(r) + \rho_{DM}(r)] 4\pi r^2 dr = 2M_\bullet, \quad (2.6)$$

where ρ_* is the density of stellar matter. For Draco we adopt from ref. [39]

$$\rho_*(r) = \rho_{*,0} \left(1 + \left(\frac{r}{b} \right)^2 \right)^{-\alpha/2}, \quad (2.7)$$

with $\alpha = 7$, $b = 0.394 \text{ kpc}$ and $\rho_{*,0} = 1.08 \times 10^7 M_\odot/\text{kpc}^3$. Using this, we find for Draco $r_h \sim 0.8 \text{ pc}$ ($r_h \sim 25 \text{ pc}$) for $M_\bullet = 10^2 M_\odot$ ($10^5 M_\odot$). For Draco (and dSphs in general) the low stellar density near the center compared to the DM density (see also figure 1) means that the difference in r_h calculated with eq. (2.4) as opposed to 2.5 is marginal (0.6% at most). We will therefor ignore the contribution of stellar matter to the radius of gravitational influence when calculating the spiked profile.

As mentioned in section 2.3, we assume the black hole grows adiabatically. This causes the surrounding DM to contract, leading to an increase in the DM density. If the BH forms and grows at the center of the DM halo, then, for an initial density profile like eq. (2.1), the spiked density profile follows [4]:

$$\rho_{\text{sp}}(r) = \rho(r_{\text{sp}}) \left(\frac{r}{r_{\text{sp}}} \right)^{-\gamma_{\text{sp}}}, \quad (2.8)$$

where the radius of the spike is $r_{\text{sp}} \approx 0.2r_h$ [40] and $\gamma_{\text{sp}} = (9-2\gamma)/(4-\gamma)$. We therefore see that γ_{sp} is a weak function of γ and for an initial NFW (with $\gamma = 1$) $r_{\text{sp}} \approx 5 \text{ pc}$ and, $\gamma_{\text{sp}} = 7/3$. The result can be easily generalised to other DM profiles.

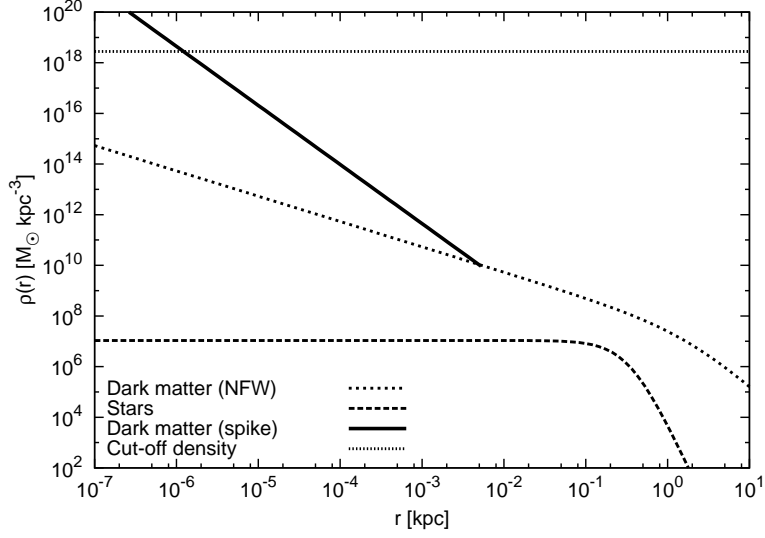


Figure 1: We show here the different density profiles of Draco as a function of radius. For this plot values of $M_{\bullet} = 10^5 M_{\odot}$, $t_{\bullet} = 10^{10}$ yr, $m_{\chi} = 100$ GeV and $\langle\sigma v\rangle = 3 \times 10^{-26} \text{ cm}^3\text{s}^{-1}$ were chosen.

Although formally divergent, a physical upper limit to the DM halo density arises for self-annihilating WIMP models:

$$\rho_{\text{lim}} \equiv \frac{m_{\chi}}{\langle\sigma v\rangle (t - t_f)} , \quad (2.9)$$

where $t - t_f = t_{\bullet}$ is the age of the halo, which for Draco we estimated to be 10^{10} yr, based on the chemical composition of its stellar population [41]. This shows that annihilations place an upper limit on the DM density of the order $m_{\chi}/\langle\sigma v\rangle(t - t_f)$, and we define r_{cut} as the radius where $\rho_{\text{sp}}(r_{\text{cut}}) = \rho_{\text{lim}}$.¹ For $m_{\chi} = 100$ GeV and $\langle\sigma v\rangle = 3 \times 10^{-26} \text{ cm}^3\text{s}^{-1}$ we find $\rho_{\text{lim}} = 1.1 \times 10^{11} \text{ GeV}/\text{cm}^3 \cong 2.8 \times 10^{18} M_{\odot}/\text{kpc}^3$ (see also figure 1) and a black hole mass of $10^5 M_{\odot}$ then gives $r_{\text{cut}} = 6.3 \times 10^{-4} \text{ pc}$.

Finally, we can express the flux of gamma-rays from a spike around an IMBH as [34]:

$$\frac{d\Phi_{\text{spike}}}{dE} \simeq \frac{1}{2} \frac{\langle\sigma v\rangle}{m_{\chi}^2} \frac{1}{D^2} \frac{dN_{\gamma}}{dE} \int_{r_{\text{cut}}}^{r_{\text{sp}}} \rho_{\text{sp}}^2(r) r^2 dr \simeq \frac{10}{3} \frac{dN_{\gamma}}{dE} \frac{\langle\sigma v\rangle}{m_{\chi}^2} \frac{\rho^2(r_{\text{sp}})}{D^2} r_{\text{sp}}^{14/3} r_{\text{cut}}^{-5/3}, \quad (2.10)$$

where in the last step we assumed $r_{\text{sp}} \gg r_{\text{cut}}$. The total flux originating from a spiked profile is the sum of the flux of the mini-spike and that of the NFW profile.

To extract the functional dependence of Φ_{sp} on M_{\bullet} , we approximate r_h by using eq. (2.5) with $\gamma = 1$. In doing so, we neglect the contribution of stars and the cusp

¹ Strictly speaking, the cut-off only appears in the case of circular DM particle orbits, see [42], in other cases a weak cusp is formed. The difference is negligible for our case.

of the NFW profile. However, these contribute little to the density at a radius on the order of $r_h \sim 10^{-3} \text{ kpc}$ (see also figure 1). Using $r_{\text{sp}} = 0.2r_h = 0.2\sqrt{M_\bullet/\pi\rho_0 r_0}$ and $r_{\text{cut}} = \left(r_{\text{sp}}^4 (\rho_0 r_0 t_\bullet/m_\chi)^3\right)^{1/7}$ and substituting these into eq. (2.10), we find

$$\Phi_{\text{spike}} \propto \frac{\langle\sigma v\rangle^{2/7}}{m_\chi^{9/7}} \frac{M_\bullet^{6/7} r_0^{3/7} \rho_0^{3/7}}{t_\bullet^{5/7}}. \quad (2.11)$$

From this, we see that, for a fixed Φ_{spike} , $\langle\sigma v\rangle \propto M_\bullet^{-3}$.

2.5 Persistence of the mini-spike

There are several possible events in the history of a dSph that could have the effect of lessening or completely erasing the density spike or preventing it from forming at all. For instance, simulations have shown that a merger of two DM halos, each containing a MBH, leads to a BH binary which ejects DM particles that pass the binary within a few times its semi-major axis [14]. In certain cases, this might even have the effect of decreasing the DM density below that of a halo without an IMBH. Other phenomena, for example the passing of a molecular cloud, open/globular cluster or the presence of a central bar would all serve to heat up the cold orbits of the DM particles in the spike, diminishing or destroying the spike [13].

Additionally, ref. [13] examined the importance of the assumptions that the BH grows adiabatically. In the case that the BH growth occurs too rapidly to be considered adiabatic (approximated by instantaneous growth of the BH), the angular momentum of an orbiting DM particle is still conserved, but its energy is not. Unlike the case of adiabatic growth, this means that an initially circular orbit does not stay circular, instead DM particles will follow elliptical, Keplerian orbits. While particles in these orbits reach smaller radii than the circular orbits in the adiabatic case, their velocities at these small radii are much larger, the result of which being that a DM particle spends most of its time at radii larger than in the adiabatic case. It follows that, while the BH still causes a density enhancement, it is much shallower than in the adiabatic case: $\rho_{\text{sp}} \propto r^{-4/3}$ for an initial NFW profile. Thus, for a non-adiabatically growing IMBH, eq. (2.10) becomes

$$\Phi_{\text{spike, non-ad.}} = \frac{3}{2} \frac{\text{d}N_\gamma}{\text{d}E} \frac{\langle\sigma v\rangle}{m_\chi^2} \frac{\rho^2(r_{\text{sp}})}{D^2} r_{\text{sp}}^3, \quad (2.12)$$

where we again use $r_{\text{cut}} \ll r_{\text{sp}}$.

In the case of an off-center (with respect to the DM halo) formation of an IMBH, like in case of the popIII scenario, the spike is also significantly shallower, with $\rho \propto r^{-3/2}$ [4, 17], and the resulting flux is given by

$$\Phi_{\text{spike, off-c.}} = \frac{1}{2} \frac{\text{d}N_\gamma}{\text{d}E} \frac{\langle\sigma v\rangle}{m_\chi^2} \frac{\rho^2(r_{\text{sp}})}{D^2} r_{\text{sp}}^3 \log \left[\frac{r_{\text{sp}}}{r_{\text{cut}}} \right]. \quad (2.13)$$

3 Intermediate mass black holes in dwarf spheroidals

Previous analyses of mini-spikes have focused on randomly generated populations of IMBHs, in the framework of specific formation scenarios, and on comparisons with gamma-ray [22, 34, 43, 44] and neutrino [18] observations. Here we consider specifically dwarf galaxies, for which halo properties are observationally known, and assume the mass of the black hole as a free parameter.

3.1 Monte Carlo simulation of merger histories

Refs. [13, 14] studied DM spikes as a result of the presence of a SMBH in the context of a MW-like galaxy, and discuss the many incidents that would disrupt a spike at the Galactic center. As noted above events that are connected to the evolution of a galaxy in hierarchical structure formation, such as BH binary mergers and rapid gas accretion on the BH would decrease the relevance of a DM spike.² To estimate the impact of BH mergers and gas accretion we develop models of the hierarchical evolution of dSph galaxies inside a MW-like galaxy, and trace their dynamical and accretion history. The models are presented in detail in ref. [46] and we summarize here their main features.

Our technique follows that of [47], as we use Monte Carlo realizations of the merger histories of DM halos. We analyze here 15 different realizations of halos that reach a mass of $M_h = 2 \times 10^{12} M_\odot$ at $z = 0$. We seed the high-redshift progenitor halos with BHs as per scenario popIII and scenario pGas and follow them from formation to $z = 0$.

For scenario popIII we assume that Pop III stars form in metal-free halos with $T_{\text{vir}} > 2000 \text{ K}$ [48], where we model metal enrichment by the ‘high feedback, best guess’ model of ref. [49]. Namely, we model metal enrichment via pair-instability supernovae winds, by following the expansion of spherical outflows into the Hubble flow and calculate the probability that a halo of mass M_h forms from metal-free gas at a redshift z . When a halo forms in our merger tree we calculate the probability that it is metal-free. If a random draw satisfies this conditions we assume a seed BH of $100 M_\odot$ forms.

For scenario pGas we rely instead on the collapse of dense gas, where we assume that gas is accumulated in the center of a halo via viscous instabilities [50, 51]. The gas inflow can be computed from the Toomre stability criterion (via the critical Toomre parameter, $Q_c \simeq 2$). This process is particularly effective for metal-free halos where cooling is driven by atomic hydrogen cooling (we test for metal enrichment of a halo as in scenario popIII). Atomic hydrogen cooling is effective in systems with $T_{\text{vir}} > 10^4 \text{ K}$, corresponding to large halos with mass $\approx 10^8 M_\odot$. The gas can cool via atomic line cooling to a temperature $T_{\text{gas}} = 5000 \text{ K}$. The efficiency of the seed assembly process ceases at large halo masses ($T_{\text{vir}} > 1.4 \times 10^4 \text{ K}$), where the mass-accretion rate from the halo is above the critical threshold for fragmentation and the disc undergoes global star formation instead. Given a DM halo with halo mass M_h , virial temperature T_{vir} , and

²For a recent discussion of a spike at the Galactic center in the context of the 1–3 GeV excess, see [45]

spin parameter λ [52], the BH mass can be expressed as [50]:

$$M_{\bullet} = f_d M_h \left[1 - \sqrt{\frac{8\lambda}{f_d Q_c} \left(\frac{j_d}{f_d} \right) \left(\frac{T_{\text{gas}}}{T_{\text{vir}}} \right)^{1/2}} \right], \quad (3.1)$$

for $\lambda < \lambda_{\text{max}} = (f_d Q_c / 8)(f_d / j_d)(T_{\text{vir}} / T_{\text{gas}})^{1/2}$. Here λ_{max} is the maximum halo spin parameter for which the disc is gravitationally unstable, $f_d \sim 0.05$ normalizes the amount of gas that participates in the infall expressed as a fraction of the halo mass, and $j_d \sim f_d$ is the fraction of the halo angular momentum retained by the collapsing gas.

Throughout the BH+halo evolution we keep track of BH-BH mergers prompted by halo mergers, and merger-driven gas inflows that can trigger rapid growth of the BH and disrupt the DM spike. We define the redshift of the latest such accretion episode as the “age” of the BH.

Finally, from the population of MW satellites that survive to $z = 0$ we have to extract those that resemble the dSphs analyzed in this paper. We define a given satellite in our simulation as dSph analog if it matches a given dSph in DM halo mass and distance from the Galactic center. This requires in the first place to model the dynamical evolution of a satellite. When a satellite enters the halo of the MW it evolves in the potential well of the host until $z = 0$, experiencing tidal stripping and possibly merging with the host. For each satellite that merges with the main halo of the merger tree, we evolve the satellite-host system by integrating the equation of motion of the satellite in the gravitational potential of the host (assuming spherical NFW profiles, [31]). In the equations of motion, we include the dynamical friction term:

$$\frac{d^2 \vec{r}}{dt^2} = -\frac{GM(r)}{r^2} \vec{r} - \frac{4\pi G^2 \ln \Lambda \rho M_{\text{sat}}}{v^2} f(x) \vec{v}, \quad (3.2)$$

where $f(x) \equiv [\text{erf}(x) - (2x/\sqrt{\pi})e^{-x^2}]$, $x \equiv v/\sqrt{2}\sigma$, and the velocity dispersion σ is derived from the Jeans’ equation for the composite density profile, assuming isotropy [53]. Here $M(r)$ describes the total mass of the host within r , $\rho(r)$ is the total density profile, and the second term represents dynamical friction against the background. We include the BH Keplerian potential if the galaxies host a BH. The Coulomb logarithm, $\ln \Lambda$, in eq. (3.2) is taken equal to 2.5 [54]. The mass of the satellite evolves during the integration because of tidal stripping. At every step of the integration we compare the mean density of the satellite to the mean density of the host halo at the location of the satellite. Tidal stripping occurs at the radius within which the mean density of the satellite exceeds the density of the galaxy interior to its orbital radius [54]. We trace the orbital evolution and the tidal stripping of all satellites from the time when the satellite enters the virial radius of the host to $z = 0$. Satellites that survive until the present time provide an analogue of the dSph population around the MW (see ref. [46] for a comparison with observational properties of the dSph population).

3.1.1 IMBHs in dwarf spheroidals of the Milky Way and M31

Given our assumptions for BH formation, not all galaxies necessarily host a BH. In the case of Draco-analogs we find *that only 18% of them host a central BH in scenario*

popIII, and 8% in scenario *pGas*. However, when we analyze the population of BHs in simulated dSph we find that many of the incidents studied by [13] and [14] that could diminish the spike in the case of the Milky-Way, e.g. DM scattering off stars, do not apply. Our simulations of Draco-like halos show 57% of BHs in scenario *popIII* and 35% in scenario *pGas* undergo BH-BH mergers, with the mean redshift since the last merger being $z = 7.2 \pm 4.0$ for scenario *popIII* and 4.3 ± 3.2 for scenario *pGas*, at $t \sim 0.8$ Gyr and $t \sim 1.4$ Gyr, respectively.

For comparison, the fraction of Ursa Minor-analogs that host a central BH are similar to Draco’s, while in the case of Ursa Major II the fractions increase to 41% and 14% in scenario *popIII* and *pGas* respectively. The fraction of BHs that experienced a BH-BH merger remains between 30% and 60%. The BH ages are also comparable to Draco’s case.

We can use our simulations to derive an estimation on the probability of a dSph in the MW or the M31 (Andromeda) galaxy containing a scenario *popIII*/*pGas* IMBH. This is done by taking a *population of 30 dSphs* similar to that of the MW (18 dSphs, as taken from [55]) and M31 (12 dSphs, from [56]) from our simulations. We consider a simulated dSph as an analog to a physical dSph if the distance to the center of its host galaxy lies within 10% of its physical counter-part. We assume all dSphs have a typical halo mass of $\sim 3 \times 10^9 M_\odot$ [57], and look for analogs with masses within a range of $3 \times 10^8 M_\odot \leq M_h \leq 3 \times 10^{10} M_\odot$. The probability of forming an IMBH via a scenario is derived by comparing the amount of simulated analogs with an IMBH to the total number of analogs.

Considering the full set of MW and M31 dwarfs, we find in the case of scenario *pGas* that the *average* probability of a dSph hosting an IMBH is 10%, of which 35%, on average, undergo a BH-BH merger. After calculating both the total probability of a BH being formed and the total probability of it surviving without a merger event, our simulations show that the probability of none of the dSphs in either the MW or Andromeda galaxy hosting an IMBH is 0.053% (3.4%) for scenario *popIII* (*pGas*), respectively (see table 2). The probability of *none* of the dSphs containing an *unmerged* BH (for which we expect an increased annihilation flux due to the mini-spike generation as discussed above) is somewhat higher and 8.5% (16%) in scenario *popIII* (*pGas*). We checked that both increasing and decreasing the assumed halo mass results in an even slightly lower probability that none of the dSphs in our simulations host an unmerged *pGas* IMBH.

	Scenario <i>popIII</i>	Scenario <i>pGas</i>
No IMBH in any dSph	5.3×10^{-4}	0.034
No unmerged IMBH in any dSph	0.085	0.16

Table 2: Total probabilities for the MW and M31 dSphs to *not* contain any (unmerged) IMBH, for both IMBH formation scenarios, as resulting from our simulations.

3.2 Other limits on the black hole mass

We will now examine two alternative methods used to derive estimates of M_\bullet ; the M_\bullet – σ relation and substructure considerations. We will compare these values to upper limits derived from gamma-rays in the next section.

3.2.1 SMBH-host galaxy relations and substructure considerations

There is an empirical relation between the mass of a SMBH and the velocity dispersion of its host galaxy. This M_\bullet – σ_* relation is obtained by fitting a sample of dynamically measured black hole masses and corresponding line-of-sight velocity dispersions to the power law

$$\log_{10} M_\bullet = \alpha + \beta \log_{10} \left[\frac{\sigma_*}{100 \text{ km s}^{-1}} \right], \quad (3.3)$$

where $\alpha = 6.91$ and $\beta = 4$ [58]. Thus, an average velocity dispersion of the stellar component for Draco of 9.1 km/s implies a M_\bullet of $557 M_\odot$. It should be noted that the behavior of the M_\bullet – σ_* relation at low M_\bullet , or whether it applies at all, is unknown.

In the case of Ursa Minor, an upper limit on M_\bullet has been derived through N-body simulations. The dwarf UMi features a dynamically cold, long-lived substructure on the northeast side of its major axis. In the case without a central IMBH, this substructure can persist long enough to explain its observation. However, the introduction of a central IMBH causes the clump to diffuse through gravitational interaction with the BH at a rate depending on the mass of the BH. If the clump is a primordial feature of UMi, its persistence imposes an upper limit of $M_\bullet = (2 - 3) \times 10^4 M_\odot$ on a central IMBH [59].

3.2.2 Kinematic measurements

We have developed kinematic models of Draco to test the ability to detect (and possibly measure) a putative BH mass through kinematic measurements. The basic idea (see refs. [60, 61] for details) is that a massive BH in a galaxy center causes gas and stars in its vicinity to move faster than they would in the presence of the galaxy potential only, as an additional Keplerian potential exists. For all galaxies other than the MW we have to rely on integrated stellar dynamics. The whole potential of the galaxy is modeled to extract the signature of the BH, from spectra of the central nucleus that provide information on the velocity dispersion integrated along the line of sight vs radius, and the stellar surface brightness. This data is used to reconstruct the underlying gravitational potential that produces a self-consistent description of the stellar system, and derive the mass density (luminous + BH + DM) which reproduces the observables. One such attempt was done on one dSph, Fornax [62], and the 1-sigma upper limit on the mass of a putative BH in Fornax is $3.2 \times 10^4 M_\odot$.

We create a simple framework that allows us to estimate the impact of a BH on the line-of-sight (LOS) velocity dispersion of Draco, and compare it to the observations [63]. We follow a procedure similar to the one described by [39] except that we treat the whole problem analytically, by solving Jeans’ equation [53, 64, 65]:

$$\frac{d(\rho_* \sigma_r^2)}{dr} + \frac{2\beta}{r} \rho_* = -\rho_* \frac{d\Phi}{dr}, \quad (3.4)$$

where $\beta(r) \equiv 1 - \sigma_t^2(r)/\sigma_r^2(r)$ is the anisotropy parameter (σ_t and σ_r are the tangential and radial velocity dispersions respectively; β equals $-\infty$, 0, and 1 for purely tangential, isotropic, and purely radial orbits respectively), and Φ is the gravitational potential.

Eq. 3.4 admits a solution of the following form:

$$\rho_* \sigma_r^2(r) = \int_r^\infty \rho_*(s) \frac{G M(< s)}{s^2} \exp \left[2 \int_r^s \frac{\beta(t) dt}{t} \right] dt. \quad (3.5)$$

Here $M(< r)$ is the mass within the radius of interest, and includes DM, stars, and cases without and with a central $10^5 M_\odot$ BH. This is a very large BH for a galaxy like Draco where the total stellar mass is $\sim 10^6 M_\odot$ (normally the BH mass is few $\sim 10^{-3}$ the bulge mass, therefore \leq few $\sim 10^{-3}$ the total stellar mass), but we want to look at the kinematic signature of an extreme case. A lower mass BH's signature would only be smaller.

We fix the DM density profile to the one given in Table 1, and we adopt a stellar density profile with the functional form given in section 2.4, but we allow the parameters, $\rho_{*,0}$ and b to vary. We consider both models with β constant with radius (as done by ref. [66]), and models with radius-dependent β , adopting the functional form suggested by [39]: $\beta = 2\eta/(1 + \eta)$, where $\eta = \eta_0 + (\eta_1 - \eta_0)[1 - (\rho_*/\rho_0)^{1/\lambda}]$, and η_0 , η_1 and λ are free parameters.

We then calculate the LOS velocity dispersion:

$$\sigma_{LOS}(R) = \frac{2}{\Sigma(R)} \int_R^\infty \left(1 - \beta \frac{R^2}{r^2} \right) \frac{\rho_* \sigma_r^2 r}{\sqrt{r^2 - R^2}} dr, \quad (3.6)$$

with Σ being the stellar surface density. It is well known that the velocity anisotropy, $\beta(r)$, is degenerate with the mass profile in determining the velocity dispersion, and that projection effects in determining the LOS velocity dispersion affect the final result. In fact, we find a large family of models with different $\rho_{*,0}$, b and $\beta(r)$ to match the data equivalently well. Additionally, as shown in fig. 2 the signature of the BH is completely invisible in today's data. Even if future measurements were to further extend to the inner radii, the difference between a case with and without BHs is sufficiently small that extracting the BH mass from the total potential may be daunting, especially because dSph galaxies have very low central stellar density, therefore very few stars that one can use as kinematic tracers [46].

4 *Fermi* LAT analysis

We will now update the upper limit derived on the gamma-ray flux from Draco that were previously presented in the literature (see e.g. ref. [55]), and discuss the impact on and the relevance for the IMBHs in scenario pGas.

4.1 Data reduction and statistical method

For our analysis we used data from the *Fermi* LAT gamma-ray space telescope. The data used was obtained between 04-08-2008 and 23-06-2014, spans an energy range of

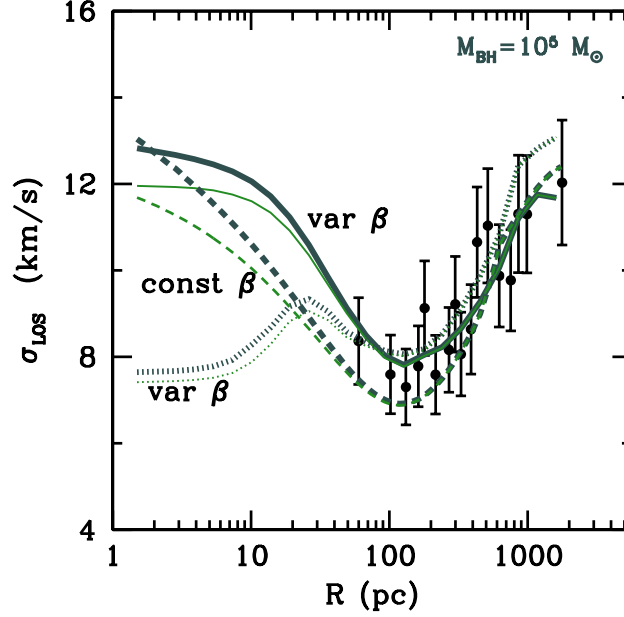


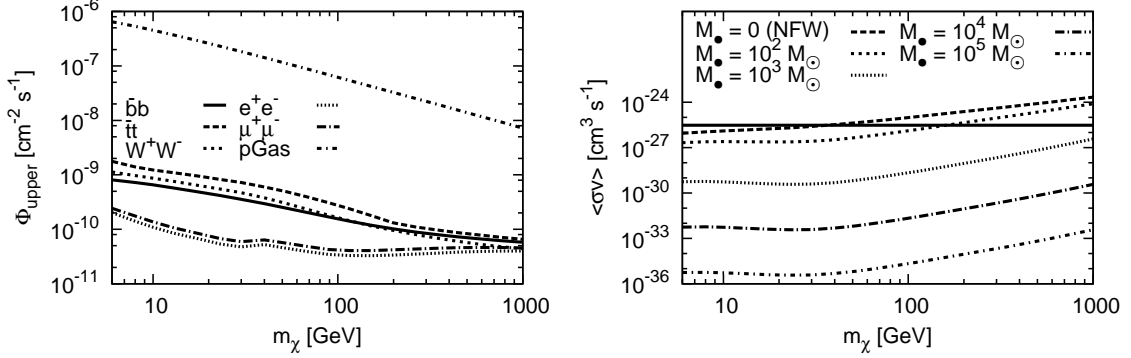
Figure 2: Line of sight velocity dispersion for Draco without (green thin curves) and with (dark gray thick curves) a central $10^5 M_\odot$ BH. The dashed curves refer to a model with anisotropy parameter, β , constant with radius ($\beta = 0.3$; $\rho_{*,0} = 10^7 M_\odot$, $b = 0.125$ kpc), the solid and dotted curves to models where β is a function of radius ($\eta_0 = 0$; $\eta_1 = 0.2$; $\lambda = 1.7$; $\rho_{*,0} = 2.5 \times 10^7 M_\odot$, $b = 0.158$ kpc and $\eta_0 = -0.8$; $\eta_1 = 0$; $\lambda = 1.3$; $\rho_{*,0} = 2 \times 10^7 M_\odot$, $b = 0.158$ respectively; for details see the text and ref. [39]).

100 MeV to 100 GeV and it encompasses a 10° radius circle centered on the coordinates of Draco; $l = 260.1^\circ$, $b = 57.9^\circ$. Using the *Fermi* Science Tools, we first applied several cuts to the data. We set the maximum zenith angle to 100° to exclude time intervals with elevated background levels caused by intersection of the region of interest with the Earth’s limb, and our cut on rocking angle $< 52^\circ$ serves the same purpose. We also excluded periods when a spacecraft event could have affected the data quality or the LAT instrument was not in normal science data-taking mode.

We used the *Fermi* Science Tools³ to perform a binned likelihood analysis, fitting the data to our different models, using twenty different WIMP masses logarithmically spaced between 6 GeV and 1000 GeV, for annihilation channels $\bar{b}b$, $\bar{t}t$, W^+W^- , e^+e^- and $\mu^+\mu^-$. For the energy spectrum dN_γ/dE for different masses and annihilation channels, we used tables provided by ref. [67]. We model Draco as a point source, with a spectrum defined by the aforementioned dN_γ/dE distribution multiplied by a normalization prefactor. Our analysis resulted in a 95% confidence level (i.e. $2\Delta\ln(\mathcal{L}) =$

³Version v9r33p0, freely available from <http://fermi.gsfc.nasa.gov/ssc/data/analysis/software/>

Figure 3



(a) Upper limits on gamma-ray flux from WIMP annihilation in Draco, for several annihilation channels. For comparison, the expected flux from annihilation into $\bar{b}b$ for a pGas IMBH ($M_\bullet = 10^5 M_\odot$) is also shown. (b) Upper limits on WIMP parameters obtained through our analysis for annihilation into $\bar{b}b$. The solid line indicates $\langle\sigma v\rangle = 3 \times 10^{-26} \text{cm}^3 \text{s}^{-1}$.

2.71 where \mathcal{L} is the likelihood) upper limit on the gamma-ray flux from Draco.

4.2 Results for Draco

4.2.1 Flux and cross section upper limits

Our results for the flux upper limits are shown in figure 3a, and are consistent with those previously obtained for example in ref. [55]. In the case of a typical scenario pGas IMBH with $M_\bullet \sim 10^5 M_\odot$, the expected flux is between 2 and 3 orders of magnitude higher than these upper limits, and thus, in the case of a standard thermal WIMP, scenario pGas IMBHs can be ruled out for all Galactic dSphs. We demonstrate this by using our derived flux upper limits to put upper limits on the cross section $\langle\sigma v\rangle$ as function of the WIMP mass m_χ and for a certain black hole mass M_\bullet . The results for the $\bar{b}b$ channel and five different black hole masses is shown in figure 3b.

4.2.2 Black hole mass upper limit

Since the annihilation flux increases in general with the mass of the IMBH, we can derive, for a fixed annihilation cross section and DM mass, upper limits on the IMBH mass. To this end, we shall consider two values for the cross section; the thermal cross section, derived from the assumption that WIMP DM is a thermal relic from the early universe, $\langle\sigma v\rangle = 3 \times 10^{-26} \text{cm}^3 \text{s}^{-1}$, and a more “pessimistic” scenario (so called because a lower cross section diminishes the prospects for indirect detection), with $\langle\sigma v\rangle = 1 \times 10^{-29} \text{cm}^3 \text{s}^{-1}$. As shown in fig. 4a, for both cross sections we rule out IMBH masses consistent with scenario pGas ($M_\bullet \sim 10^5 M_\odot$).

Note that, in figure 4a, the cut-off is caused by the fact that even the case for $M_\bullet = 0$ (i.e. the unmodified NFW profile) is ruled out at $\langle\sigma v\rangle = 3 \times 10^{-26} \text{cm}^3 \text{s}^{-1}$ for

Figure 4: A comparison of the upper limits on black hole mass M_\bullet in Draco as a function of WIMP mass m_χ for the different cases we considered.

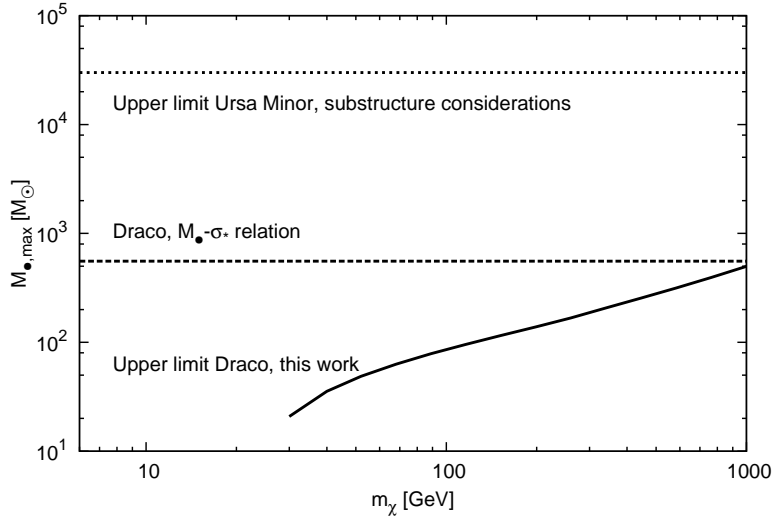
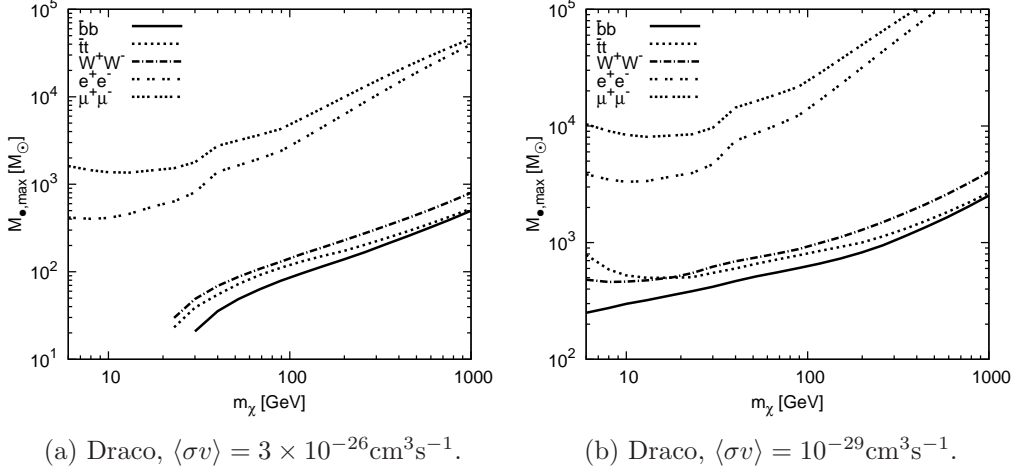
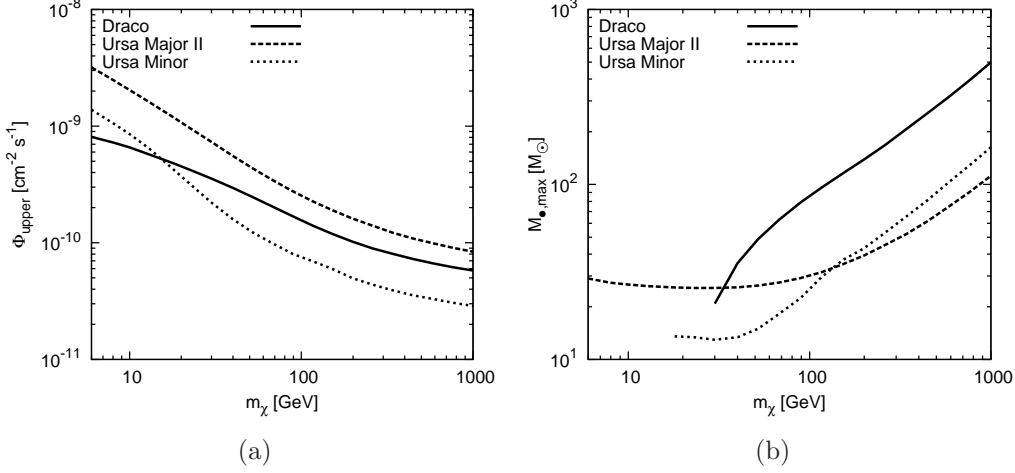


Figure 5: Upper limit on the mass of the IMBH for Draco derived in this work from annihilation into $\bar{b}b$, compared to the IMBH mass expected from the M_\bullet - σ_* relation.

$m_\chi \lesssim 40$ GeV for the $\bar{b}b$ channel, as can be seen in figure 3b. In contrast, the horizontal asymptotic behavior in figure 4b is caused by the flattening of $\langle\sigma v\rangle$ - m_χ at low WIMP mass (see also figure 3b).

Our upper limits on M_\bullet that we obtained from Fermi LAT observations and the WIMP hypothesis are stronger than those that we derived from the methods described above in section 3.2.1, as can be seen in figure 5.

Figure 6: Upper limits on gamma-ray flux (6a) and black hole mass M_\bullet (6b) for Ursa Minor and Ursa Major II as a function of WIMP mass m_χ , in comparison to Draco, for the $b\bar{b}$ channel and a thermal cross section.



Recently, the mini-spike scenario was used along with IMBH masses derived from, amongst others, the M_\bullet - σ_* relation to derive constraints on WIMPs [68], and these results are consistent with ours. From our results it can be seen that the thermal WIMP scenario rules out IMBH masses derived from the M_\bullet - σ_* relation for Draco, for WIMP masses < 1 TeV.

We note that in the case of either non-adiabatic growth or off-center formation (see section 2.5), our constraints become much looser; $M_\bullet \lesssim 10^7$ – $10^8 M_\odot$.

4.3 Other dwarf spheroidal galaxies

Considering heliocentric distance and expected J-factor, the two next best candidates after Draco for detection of gamma-rays from DM annihilation appear to be the Ursa Minor and Ursa Major II dSphs (see table 1). To check for consistency, we repeat our analysis for these objects. Our results for Φ_{upper} and $M_{\bullet, \text{max}}$ in the thermal relic and $t_\bullet = 10^{10}$ yr case for Ursa Minor and Ursa Major II are shown in figure 6, and are comparable to the results previously obtained for Draco.

We can use known upper limits on the gamma-ray flux from nearly *all* Galactic dSphs (specifically, 18 dSphs), as derived in ref. [55], to infer general limits on IMBHs in scenario pGas. As mentioned in section 4.2.1, the presence of a mini-spike originating from the formation of a scenario pGas IMBH would cause the expected gamma-ray flux from Draco to overshoot the upper limits by 2 to 3 orders of magnitude. Given that from both, our comparison of Ursa Minor and Ursa Major II to Draco as well as already known results [55], the flux upper limits for the various Galactic dSph are at the same order of magnitude, and given that the expected flux from a mini-spike does not depend strongly on the parameters of the original NFW profile of the dSph (see eq. (2.11)), we

conclude that the existence of scenario pGas IMBHs without previous BH-BH merger is ruled out for all Galactic dSphs mentioned in ref. [55].

We can extend this argument to dSphs in M31, though there are currently no upper limits on the gamma-ray flux from these objects. In section 3.1.1, we selected a population of 12 M31 dSphs with an average heliocentric distance of 711 kpc. Since the measured flux scales with the inverse of distance squared, we can rescale the upper limits derived for e.g. Draco to the case of an M31 dSph: $76^2/711^2 \simeq 0.01$, meaning that the expected boost in flux of 2–3 orders of magnitude would still be visible in M31 dSphs. It is hence plausible that also M31 dSphs do not harbor any unmerged IMBH from scenario pGas.

Finally, we remind that in our above Monte Carlo simulations of the BH merger history we inferred that in the case of scenario pGas the chances of none of the MW and M31 dSphs harboring an unmerged IMBH is 16%. We hence find that—if DM is made out of WIMPs with typical masses and cross sections—scenario pGas is in slight tension with the existing gamma-ray data at about 84% CL.

5 Conclusions

We have derived constraints on the existence of IMBHs in dwarf spheroidal galaxies, focusing in particular on the case where DM is made of WIMPs with typical masses and self-annihilation cross sections. We focused in particular on a formation scenario, pGas, where IMBH originate from massive objects formed directly during the collapse of primordial gas in early-forming halos (with $M_\bullet \sim 10^5 M_\odot$). IMBH generated by the collapse of Pop III stars are unlikely to feature surviving mini-spikes.

Using almost 6 years of *Fermi* LAT data we determined an upper limit on the DM annihilation flux (figure 3a) and cross section (figure 3b) as a function of WIMP mass for five different annihilation channels from dSphs Draco, Ursa Minor and Ursa Major II, which we modeled as point sources with a DM distribution following a spiked NFW profile. With these flux upper limits we were then able to derive upper limits on the mass of a central IMBH in the mini-spike scenario for different annihilation cross sections (figure 4).

Our conclusions are as follows:

- Under the assumption that the IMBH grew adiabatically at the center of the dSph, we effectively rule out the existence of thermal WIMPs mini-spikes for IMBH masses $M_\bullet \gtrsim 10^3 M_\odot$ for the Draco, Ursa Minor and Ursa Major II dSphs with high significance (figures 4a, 6b).
- Our constraints on the IMBH mass M_\bullet are stronger than previous constraints derived with other methods, e.g. the $M_\bullet - \sigma_*$ relation or substructure considerations (figure 5)
- Our Monte Carlo simulations of merger histories of BH in dSphs in the pGas IMBH formation scenario indicate that, while the probability of an individual dSph

hosting an IMBH is quite low (about 10%), it is somewhat unlikely (probability 16%) that *none* of the dSph satellites of the MW and M31 host such an IMBH with a surviving mini-spike.

- Given the fact that under the thermal WIMPs hypothesis IMBHs without previous merger (and hence a surviving mini-spike) and with a mass of $\sim 10^5 M_\odot$ can be plausibly excluded for *all* of the MW and M31 dSphs, we find that scenario pGas is disfavoured by existing gamma-ray data at about 84% CL.

Acknowledgement We thank S. Profumo and A. X. Gonzalez-Morales for providing additional information on their recent work [68], which allowed a detailed comparison of our results. GB acknowledges support from the European Research Council through the ERC Starting Grant *WIMPs Kairos*

References

- [1] P. J. E. Peebles, *Star Distribution Near a Collapsed Object*, ApJ **178** (Dec., 1972) 371–376.
- [2] G. D. Quinlan, L. Hernquist, and S. Sigurdsson, *Models of Galaxies with Central Black Holes: Adiabatic Growth in Spherical Galaxies*, *Astrophys.J.* **440** (1995) 554–564, [[astro-ph/9407005](#)].
- [3] G. Bertone, ed., *Particle Dark Matter: Observations, Models and Searches*. Cambridge University Press, 2010.
- [4] P. Gondolo and J. Silk, *Dark Matter Annihilation at the Galactic Center*, *Physical Review Letters* **83** (Aug., 1999) 1719–1722, [[astro-ph/9906391](#)].
- [5] G. Jungman, M. Kamionkowski, and K. Griest, *Supersymmetric dark matter*, *Phys.Rept.* **267** (1996) 195–373, [[hep-ph/9506380](#)].
- [6] L. Bergstrom, *Nonbaryonic dark matter: Observational evidence and detection methods*, *Rept.Prog.Phys.* **63** (2000) 793, [[hep-ph/0002126](#)].
- [7] G. Bertone, D. Hooper, and J. Silk, *Particle dark matter: evidence, candidates and constraints*, *Phys. Rep.* **405** (Jan., 2005) 279–390, [[hep-ph/0404175](#)].
- [8] P. Gondolo, *Either neutralino dark matter or cuspy dark halos*, *Phys.Lett.* **B494** (2000) 181–186, [[hep-ph/0002226](#)].
- [9] G. Bertone, G. Sigl, and J. Silk, *Astrophysical limits on massive dark matter*, *Mon.Not.Roy.Astron.Soc.* **326** (2001) 799–804, [[astro-ph/0101134](#)].
- [10] G. Bertone, G. Sigl, and J. Silk, *Annihilation radiation from a dark matter spike at the galactic center*, *Mon.Not.Roy.Astron.Soc.* **337** (2002) 98, [[astro-ph/0203488](#)].
- [11] E.-J. Ahn, G. Bertone, and D. Merritt, *Impact of astrophysical processes on the gamma-ray background from dark matter annihilations*, *Phys.Rev.* **D76** (2007) 023517, [[astro-ph/0703236](#)].
- [12] A. Belikov and J. Silk, *Diffuse Gamma Ray Background from Annihilating Dark Matter in Density Spikes around Supermassive Black Holes*, *Phys.Rev.* **D89** (2014) 043520, [[arXiv:1312.0007](#)].

- [13] P. Ullio, H. Zhao, and M. Kamionkowski, *Dark-matter spike at the galactic center?*, Phys. Rev. D **64** (Aug., 2001) 043504, [[astro-ph/0101481](#)].
- [14] D. Merritt, M. Milosavljević, L. Verde, and R. Jimenez, *Dark Matter Spikes and Annihilation Radiation from the Galactic Center*, Physical Review Letters **88** (May, 2002) 191301, [[astro-ph/0201376](#)].
- [15] G. Bertone and D. Merritt, *Dark Matter Dynamics and Indirect Detection*, Modern Physics Letters A **20** (2005) 1021–1036, [[astro-ph/0504422](#)].
- [16] D. R. Pasham, T. E. Strohmayer, and R. F. Mushotzky, *A 400-solar-mass black hole in the galaxy M82*, Nature **513** (Sept., 2014) 74–76.
- [17] H. Zhao and J. Silk, *Dark Minihalos with Intermediate Mass Black Holes*, Physical Review Letters **95** (June, 2005) 011301, [[astro-ph/0501625](#)].
- [18] G. Bertone, *Prospects for detecting dark matter with neutrino telescopes in intermediate mass black holes scenarios*, Phys.Rev. **D73** (2006) 103519, [[astro-ph/0603148](#)].
- [19] M. Fornasa and G. Bertone, *Black Holes as Dark Matter Annihilation Boosters*, Int.J.Mod.Phys. **D17** (2008) 1125–1157, [[arXiv:0711.3148](#)].
- [20] **HESS Collaboration** Collaboration, F. Aharonian et al., *Search for Gamma-rays from Dark Matter annihilations around Intermediate Mass Black Holes with the H.E.S.S. experiment*, Phys.Rev. **D78** (2008) 072008, [[arXiv:0806.2981](#)].
- [21] M. Taoso, S. Ando, G. Bertone, and S. Profumo, *Angular correlations in the cosmic gamma-ray background from dark matter annihilation around intermediate-mass black holes*, Phys.Rev. **D79** (2009) 043521, [[arXiv:0811.4493](#)].
- [22] T. Bringmann, J. Lavalle, and P. Salati, *Intermediate Mass Black Holes and Nearby Dark Matter Point Sources: A Myth-Buster*, Phys.Rev.Lett. **103** (2009) 161301, [[arXiv:0902.3665](#)].
- [23] G. Bertone, M. Fornasa, M. Taoso, and A. R. Zentner, *Dark Matter Annihilation around Intermediate Mass Black Holes: an update*, New J.Phys. **11** (2009) 105016, [[arXiv:0905.4736](#)].
- [24] M. Safonova and P. Shastri, *Extrapolating SMBH correlations down the mass scale: the case for IMBHs in globular clusters*, Ap&SS **325** (Jan., 2010) 47–58, [[arXiv:0910.2551](#)].
- [25] M. L. M. Collins, S. C. Chapman, R. M. Rich, R. A. Ibata, N. F. Martin, M. J. Irwin, N. F. Bate, G. F. Lewis, J. Peñarrubia, N. Arimoto, C. M. Casey, A. M. N. Ferguson, A. Koch, A. W. McConnachie, and N. Tanvir, *The Masses of Local Group Dwarf Spheroidal Galaxies: The Death of the Universal Mass Profile*, ApJ **783** (Mar., 2014) 7, [[arXiv:1309.3053](#)].
- [26] **Fermi LAT** Collaboration, A. A. Abdo, M. Ackermann, M. Ajello, W. B. Atwood, L. Baldini, J. Ballet, G. Barbiellini, D. Bastieri, K. Bechtol, and et al., *Observations of Milky Way Dwarf Spheroidal Galaxies with the Fermi-Large Area Telescope Detector and Constraints on Dark Matter Models*, ApJ **712** (Mar., 2010) 147–158, [[arXiv:1001.4531](#)].
- [27] M. L. Mateo, *Dwarf Galaxies of the Local Group*, ARA&A **36** (1998) 435–506, [[astro-ph/9810070](#)].
- [28] J. S. Gallagher, G. J. Madsen, R. J. Reynolds, E. K. Grebel, and T. A. Smecker-Hane, *A Search for Ionized Gas in the Draco and Ursa Minor Dwarf Spheroidal Galaxies*, ApJ **588** (May, 2003) 326–330, [[astro-ph/0301228](#)].

- [29] J. Grcevich and M. E. Putman, *H I in Local Group Dwarf Galaxies and Stripping by the Galactic Halo*, ApJ **696** (May, 2009) 385–395, [[arXiv:0901.4975](#)].
- [30] M. Ségall, R. A. Ibata, M. J. Irwin, N. F. Martin, and S. Chapman, *Draco, a flawless dwarf galaxy*, MNRAS **375** (Mar., 2007) 831–842, [[astro-ph/0612263](#)].
- [31] J. F. Navarro, C. S. Frenk, and S. D. M. White, *A Universal Density Profile from Hierarchical Clustering*, ApJ **490** (Dec., 1997) 493, [[astro-ph/9611107](#)].
- [32] D. A. Swartz, K. K. Ghosh, A. F. Tennant, and K. Wu, *The Ultraluminous X-Ray Source Population from the Chandra Archive of Galaxies*, ApJS **154** (Oct., 2004) 519–539, [[astro-ph/0405498](#)].
- [33] M. Volonteri, *Formation of supermassive black holes*, A&A Rev. **18** (July, 2010) 279–315, [[arXiv:1003.4404](#)].
- [34] G. Bertone, A. R. Zentner, and J. Silk, *New signature of dark matter annihilations: Gamma rays from intermediate-mass black holes*, Phys. Rev. D **72** (Nov., 2005) 103517, [[astro-ph/0509565](#)].
- [35] P. Madau and M. J. Rees, *Massive Black Holes as Population III Remnants*, ApJ **551** (Apr., 2001) L27–L30, [[astro-ph/0101223](#)].
- [36] A. Heger, C. L. Fryer, S. E. Woosley, N. Langer, and D. H. Hartmann, *How Massive Single Stars End Their Life*, ApJ **591** (July, 2003) 288–300, [[astro-ph/0212469](#)].
- [37] S. M. Koushiappas, J. S. Bullock, and A. Dekel, *Massive black hole seeds from low angular momentum material*, MNRAS **354** (Oct., 2004) 292–304, [[astro-ph/0311487](#)].
- [38] S. L. Shapiro, S. A. Teukolsky, and A. P. Lightman, *Black Holes, White Dwarfs, and Neutron Stars: The Physics of Compact Objects*, *Physics Today* **36** (1983) 89.
- [39] S. Mashchenko, A. Sills, and H. M. Couchman, *Constraining Global Properties of the Draco Dwarf Spheroidal Galaxy*, ApJ **640** (Mar., 2006) 252–269, [[astro-ph/0511567](#)].
- [40] D. Merritt, *Single and Binary Black Holes and their Influence on Nuclear Structure, Coevolution of Black Holes and Galaxies* (2004) 263, [[astro-ph/0301257](#)].
- [41] V. Castellani, *On the age of the Draco dwarf galaxy*, MNRAS **172** (Sept., 1975) 59P–64P.
- [42] E. Vasiliev, *Dark matter annihilation near a black hole: Plateau versus weak cusp*, Phys. Rev. D **76** (Nov., 2007) 103532, [[arXiv:0707.3334](#)].
- [43] M. Fornasa, M. Taoso, and G. Bertone, *Gamma-Rays from Dark Matter Mini-Spikes in M31*, *Phys.Rev.* **D76** (2007) 043517, [[astro-ph/0703757](#)].
- [44] G. Bertone, M. Fornasa, M. Taoso, and A. R. Zentner, *Dark matter annihilation around intermediate mass black holes: an update*, *New Journal of Physics* **11** (Oct., 2009) 105016, [[arXiv:0905.4736](#)].
- [45] B. D. Fields, S. L. Shapiro, and J. Shelton, *Galactic Center Gamma-Ray Excess from Dark Matter Annihilation: Is There A Black Hole Spike?*, *ArXiv e-prints* (June, 2014) [[arXiv:1406.4856](#)].
- [46] S. van Wassenhove, M. Volonteri, M. G. Walker, and J. R. Gair, *Massive black holes lurking in Milky Way satellites*, MNRAS **408** (Oct., 2010) 1139–1146, [[arXiv:1001.5451](#)].
- [47] M. Volonteri, F. Haardt, and P. Madau, *The Assembly and Merging History of Supermassive Black Holes in Hierarchical Models of Galaxy Formation*, ApJ **582** (Jan., 2003) 559–573.

- [48] N. Yoshida, K. Omukai, L. Hernquist, and T. Abel, *Formation of Primordial Stars in a Λ CDM Universe*, *ApJ* **652** (Nov., 2006) 6–25, [[astro-ph/](#)].
- [49] E. Scannapieco, R. Schneider, and A. Ferrara, *The Detectability of the First Stars and Their Cluster Enrichment Signatures*, *ApJ* **589** (May, 2003) 35–52, [[astro-ph/0301628](#)].
- [50] G. Lodato and P. Natarajan, *Supermassive black hole formation during the assembly of pre-galactic discs*, *MNRAS* **371** (Oct., 2006) 1813–1823, [[astro-ph/](#)].
- [51] M. Volonteri, G. Lodato, and P. Natarajan, *The evolution of massive black hole seeds*, *MNRAS* **383** (Jan., 2008) 1079–1088, [[0709.0529](#)].
- [52] H. J. Mo, S. Mao, and S. D. M. White, *The formation of galactic discs*, *MNRAS* **295** (Apr., 1998) 319–336.
- [53] J. Binney and S. Tremaine, *Galactic Dynamics: Second Edition*. Galactic Dynamics: Second Edition, by James Binney and Scott Tremaine. ISBN 978-0-691-13026-2 (HB). Published by Princeton University Press, Princeton, NJ USA, 2008., 2008.
- [54] J. E. Taylor and A. Babul, *The Dynamics of Sinking Satellites around Disk Galaxies: A Poor Man’s Alternative to High-Resolution Numerical Simulations*, *ApJ* **559** (Oct., 2001) 716–735, [[astro-ph/](#)].
- [55] **Fermi LAT** Collaboration, M. Ackermann, A. Albert, B. Anderson, L. Baldini, and et al., *Dark Matter Constraints from Observations of 25 Milky Way Satellite Galaxies with the Fermi Large Area Telescope*, *ArXiv e-prints* (Oct., 2013) [[arXiv:1310.0828](#)].
- [56] E. J. Tollerud, R. L. Beaton, M. C. Geha, and et al., *The SPLASH Survey: Spectroscopy of 15 M31 Dwarf Spheroidal Satellite Galaxies*, *ApJ* **752** (June, 2012) 45, [[arXiv:1112.1067](#)].
- [57] J. Wolf, G. D. Martinez, J. S. Bullock, M. Kaplinghat, M. Geha, R. R. Muñoz, J. D. Simon, and F. F. Avedo, *Accurate masses for dispersion-supported galaxies*, *MNRAS* **406** (Aug., 2010) 1220–1237, [[arXiv:0908.2995](#)].
- [58] S. Tremaine, K. Gebhardt, R. Bender, G. Bower, A. Dressler, S. M. Faber, A. V. Filippenko, R. Green, C. Grillmair, L. C. Ho, J. Kormendy, T. R. Lauer, J. Magorrian, J. Pinkney, and D. Richstone, *The Slope of the Black Hole Mass versus Velocity Dispersion Correlation*, *ApJ* **574** (Aug., 2002) 740–753, [[astro-ph/0203468](#)].
- [59] V. Lora, F. J. Sánchez-Salcedo, A. C. Raga, and A. Esquivel, *An Upper Limit on the Mass of the Black Hole in Ursa Minor Dwarf Galaxy*, *ApJ* **699** (July, 2009) L113–L117, [[arXiv:0906.0951](#)].
- [60] L. Ferrarese and H. Ford, *Supermassive Black Holes in Galactic Nuclei: Past, Present and Future Research*, *Space Science Reviews* **116** (Feb., 2005) 523–624, [[astro-ph/0411247](#)].
- [61] J. Kormendy and L. C. Ho, *Coevolution (Or Not) of Supermassive Black Holes and Host Galaxies*, *ARA&A* **51** (Aug., 2013) 511–653, [[arXiv:1304.7762](#)].
- [62] J. R. Jardel and K. Gebhardt, *The Dark Matter Density Profile of the Fornax Dwarf*, *ApJ* **746** (Feb., 2012) 89, [[arXiv:1112.0319](#)].
- [63] M. G. Walker, M. Mateo, E. W. Olszewski, O. Y. Gnedin, X. Wang, B. Sen, and M. Woodroffe, *Velocity Dispersion Profiles of Seven Dwarf Spheroidal Galaxies*, *ApJ* **667** (Sept., 2007) L53–L56, [[arXiv:0708.0010](#)].

- [64] J. Binney and G. A. Mamon, *M/L and velocity anisotropy from observations of spherical galaxies, or must M87 have a massive black hole*, MNRAS **200** (July, 1982) 361–375.
- [65] E. L. Lokas and G. A. Mamon, *Dark matter distribution in the Coma cluster from galaxy kinematics: breaking the mass-anisotropy degeneracy*, MNRAS **343** (Aug., 2003) 401–412, [[astro-ph/0302461](#)].
- [66] **Fermi LAT** Collaboration, A. A. Abdo, M. Ackermann, M. Ajello, and et al., *Spectrum of the isotropic diffuse gamma-ray emission derived from first-year fermi large area telescope data*, *Phys. Rev. Lett.* **104** (Mar, 2010) 101101.
- [67] M. Cirelli, G. Corcella, A. Hektor, G. Hütsi, M. Kadastik, P. Panci, M. Raidal, F. Sala, and A. Strumia, *PPPC 4 DM ID: a poor particle physicist cookbook for dark matter indirect detection*, J. Cosmology Astropart. Phys. **3** (Mar., 2011) 51, [[arXiv:1012.4515](#)].
- [68] A. X. Gonzalez-Morales, S. Profumo, and F. S. Queiroz, *The Effect of Black Holes in Local Dwarf Spheroidal Galaxies on Gamma-Ray Constraints on Dark Matter Annihilation*, *ArXiv e-prints* (June, 2014) [[arXiv:1406.2424](#)].